
STRUCTURAL
CHEMISTRY

**Volume 75 (2019)**

**Supporting information for article:**

# Analysis of solvent-accessible voids and proton-coupled electron transfer of 2,6-bis(1*H*-imidazol-2-yl)pyridine and its hydrochloride

**Renan B. Guerra, Luis S. C. Huamaní, Juan C. Tenorio, Willian M. Guimarães, Juliano A. Bonacin and André Luiz Barboza Formiga**

# Analysis of solvent accessible voids and proton-coupled electron transfer of 2,6-bis(1H-imidazol-2-yl)pyridine and its hydrochloride

Authors

**Renan B. Guerra[a], Luis S. C. Huamaní[a], Juan C. Tenorio[a], Willian M. Guimarães[a], Juliano A. Bonacin[a] and André Luiz Barboza Formiga[a]***

[a]Inorganic chemistry, University of Campinas – UNICAMP, 6154, Campinas, São Paulo, 13083-970, Brazil.

Correspondence email: formiga@unicamp.br

## S1. $H_2$dimpy synthesis details and characterization

### S1.1. Materials and apparatus

2,6-pyridinecarbonitrile (97%), aminoacetaldehyde diethyl acetal (98%), sodium methoxide (NaOMe 25 wt.% in methanol), sodium hydroxide pellets (NaOH ≥ 98%), potassium chloride (KCl ≥ 99%) and potassium nitrate ($KNO_3$ ≥ 99%) were purchased from Sigma-Aldrich. Hydrochloric acid solution ($HCl_{(aq)}$ 37%) was purchased from Merck, methanol (MeOH, HPLC-grade) from Tedia (Fairfield, OH, USA) and glacial acetic acid (AcOH ≥ 99%) and diethyl ether ($Et_2O$ ≥ 99%) were purchased from LabSynth, Brazil. All reactants and solvents were used as received without further purification. MilliQ water (Millipore Corporation, USA) was used in all experiments in aqueous media.

Carbon, hydrogen and nitrogen (CHN) composition was determined by elemental analysis, carried out in a Perkin Elmer 2400 micro-analyser model using a mass sample of about 2 mg.

All the NMR spectra were obtained from 15 mg of $H_2$dimpy in 0.75 mL deuterated DMSO-$d_6$ 99.9 atom %D, using a Bruker Avance III 400 MHz spectrometer with a $^1$H frequency of 400.1800 MHz and a $^{13}$C frequency of 100.6253 MHz. The $^1$H-$^1$H COSY (correlation spectroscopy) spectrum was acquired with a 5319.1 Hz (13.29 ppm) processing spectral width in both dimensions using 2048×256 points and processed using 4096×1024 points. The $^1$H–$^{13}$C HSQC (heteronuclear single quantum coherence) spectrum were acquired using a 5376.3 Hz (13.4 ppm) processing spectral width in F2 and a 16668.7 Hz (165.63 ppm) spectral width in F1, using 2048×256 points, and processed to 4096×1024 points.

UV-Vis spectra were obtained using a Bel UV-M51 spectrophotometer with tungsten and deuterium lamps (190-1100 nm) with detection by photodiodes, performed in quartz cuvettes with an optical path length of 10.00 mm using an $H_2$dimpy concentration of $2.8\times10^{-5}$ M in different solvents.

Excitation and emission spectra were obtained with a Cary Eclipse fluorescence spectrophotometer (Varian) using a quartz cuvette of four clear windows and optical path length of 1.0 cm, using a $2.5\times10^{-5}$ M $H_2$dimpy methanolic solution. The excitation wavelength was set in 345 nm and emission detection from 340 to 500 nm, with a 5 nm slit width and a scan speed set to medium.

DSC curve was obtained using a DSC 1 system (Mettler Toledo) under the following experimental conditions: aluminum crucible with perforated cover (40 mL); the heating rate of 10 °C $min^{-1}$; nitrogen atmosphere at 50 mL $min^{-1}$ flow; and sample mass of about 3.46 mg.

The Fourier transformed infrared-attenuated total reflectance (FTIR-ATR) spectrum was run on a Cary 630 FTIR spectrophotometer (Agilent Technologies, USA) using a diamond ATR accessory with ZnSe window, within the 4000–400 $cm^{-1}$ range in transmission mode with 64 scans and resolution of 4 $cm^{-1}$.

For spectrophotometric p$K_a$ determination, 100 mL of $H_2$dimpy $3.5\times10^{-5}$ mol $L^{-1}$ in aqueous solution (5% methanol) was prepared as a stock solution. To make sure that the concentration of $H_2$dimpy would be constant through all the measurements, 25 mL of HCl 0.05 mol $L^{-1}$ and NaOH 0.05 mol $L^{-1}$ were prepared using the stock solution. Two titrations were performed with the addition of the acid and base solutions with a micropipette, recording a spectrum after each addition and pH change.

For spectroelectrochemical measurement, the Metrohm Autolab PGSTAT12 potentiostat was used with a diode array HP Agilent 8453 spectrophotometer that can work in the 190-1100 nm range and record two spectra per second. The working electrode, in this case, was a platinum grid electrode, with a standard calomel electrode (SCE) as a reference electrode, a Pt wire as an auxiliary electrode and with a 1mm optical path length for the electrochemical cell. A $3.5\times10^{-4}$ mol $L^{-1}$ solution of $H_2$dimpy was prepared using 0.1 mol $L^{-1}$ KCl as electrolyte instead of $KNO_3$ due to the strong UV absorption by the $KNO_3$.

### S1.2. $H_2$dimpy synthesis

The synthesis of 2,6-bis(1H-imidazol-2-yl)pyridine ($H_2$dimpy) was performed following procedures described in the literature (Voss *et al.*, 2008; Hashiguchi *et al.*, 2010; Rigsby *et al.*, 2012). In a round bottom flask of 100 mL, 2.582 g (20 mmol) of 2,6-pyridinecarbonitrile, 25 mL of methanol and 0.915 mL of a 30% methanolic solution of sodium methoxide (4 mmol, 0.2 eq.) were added and left under stirring for 2 hours at room temperature. Then, 5.935 mL of aminoacetaldehyde diethyl acetal (40 mmol, 2 eq.) and 2.313 mL of glacial acetic acid (40 mmol, 2 eq.) were added to the solution dropwise, followed by stirring for 1 hour and a half at 50 °C. After cooling the resulting solution at room temperature, 20 mL of methanol and 10 mL of aqueous hydrochloric acid solution (6 mol $L^{-1}$) were added and the reaction was left under stirring and reflux for 10 hours. Volatiles were then removed on the rotary evaporator and the residue was dissolved in 50 mL of $H_2O$. The resulting aqueous solution was washed 3 times with 50 mL of $Et_2O$ using a separatory funnel and the organic layer discarded. To

the resulting aqueous layer, 50 mL of $H_2O$ was added and the pH was adjusted to approximately 9 with the addition of NaOH 2 mol $L^{-1}$, followed by the precipitation of a white solid. The obtained white solid was filtered and washed with $Et_2O$ (3 × 25 mL) and the product dried under reduced pressure at 100 ºC for 3 hours. Then, the resulting product was suspended in 50 mL of $Et_2O$ and sonicated for 10 minutes, followed by filtration and washed again with $Et_2O$ (10 × 10 mL). The final product was then macerated and dried under reduced pressure overnight to afford a light yellow solid with a yield of 78% (3.29 g).

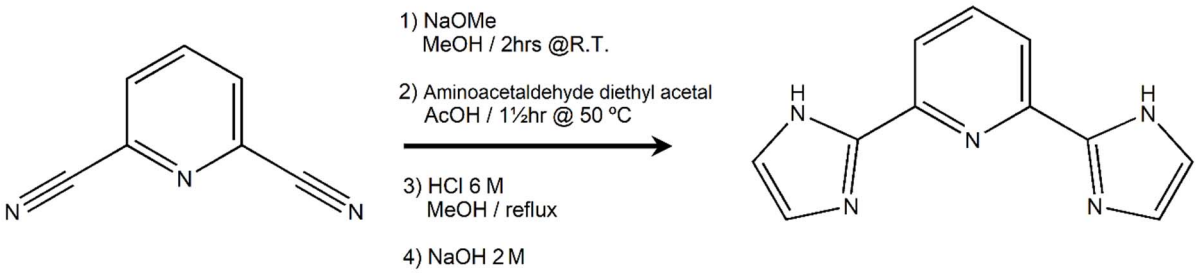


Elem. Anal. (CHN) for $C_{11}H_9N_5$: % = calculated: C, 62.55; H, 4.29; N, 33.16; found: C, 62.69; H 4.57; N, 33.07. FTIR: ATR/$cm^{-1}$ = 3409(w), 3100 (w), 1595 (m), 1558 (m), 1471 (s), 1363 (m), 1152 (m), 1079 (m), 951 (m), 812y (m), 743 (s), 649 (m), 529 (m), 440 (m). UV-vis: $\lambda_{max}$/nm (ε/ L $mol^{-1}$ $cm^{-1}$) = in MeOH 278 (26700), 319 (16900); in $H_2O$: 274 (24370), 317 (16925). Melting point (DSC): 291.6 ºC. $^1$H-NMR (400 MHz, DMSO-$d_6$, 25 ºC) δ/ppm = 12.67 (s, 2H), 7.94 (m, 1H), 7.88 (m, 2H), 7.49 (dd, J = 1.88, 1.08 Hz, 2H), 7.14 (dd, J = 1.20 Hz, 2H). $^{13}$C-NMR (100 MHz, DMSO-$d_6$, 25 ºC) δ/ppm = 148.17, 146.14, 139.02, 130.34, 118.93, 117.84.

### S1.3. $H_2$dimpy characterization

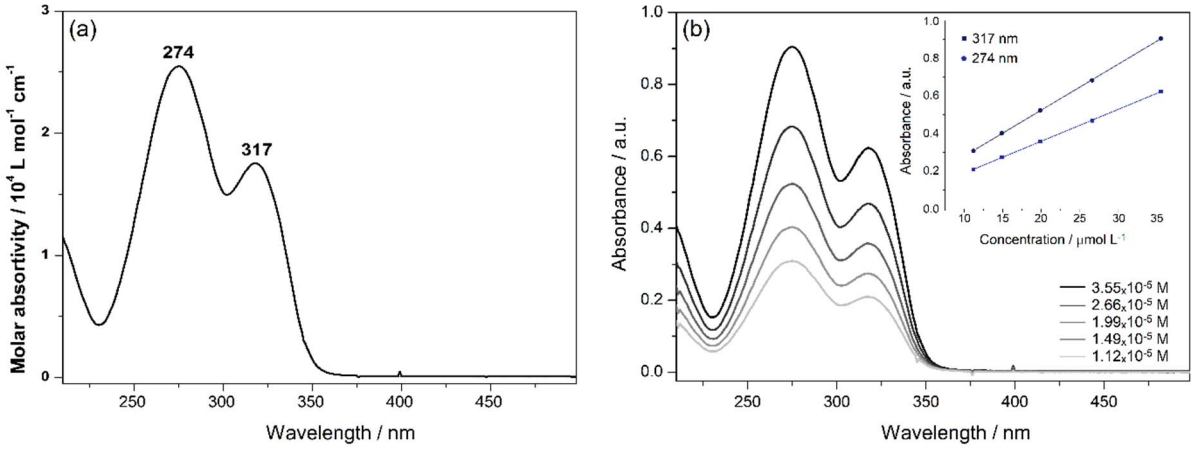


**Figure S1** UV-vis absorption spectra of $H_2$dimpy in aqueous solutions *(a)* extinction coefficients and *(b)* in different concentrations.

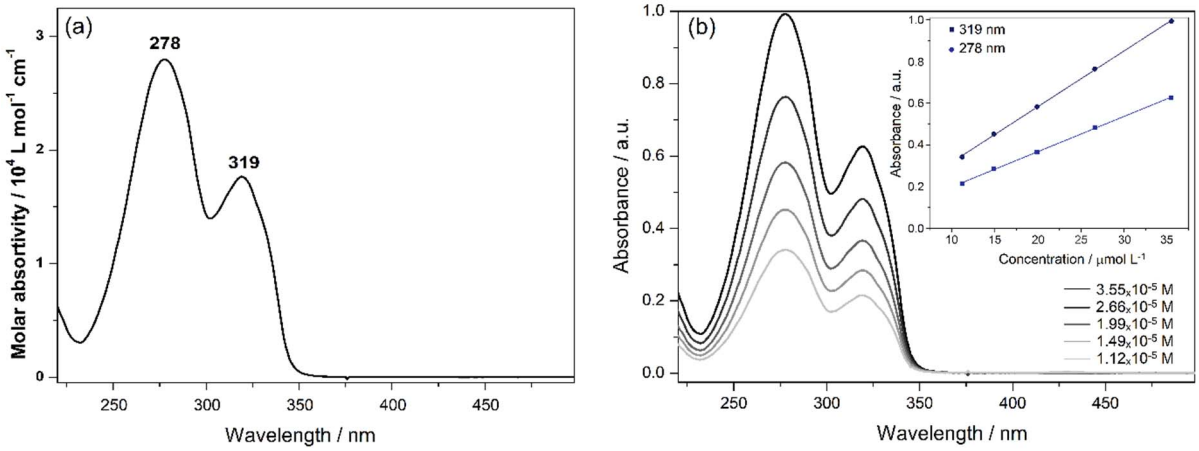


**Figure S2** UV-vis absorption spectra of $H_2$dimpy in methanol *(a)* extinction coefficients and *(b)* in different concentrations.

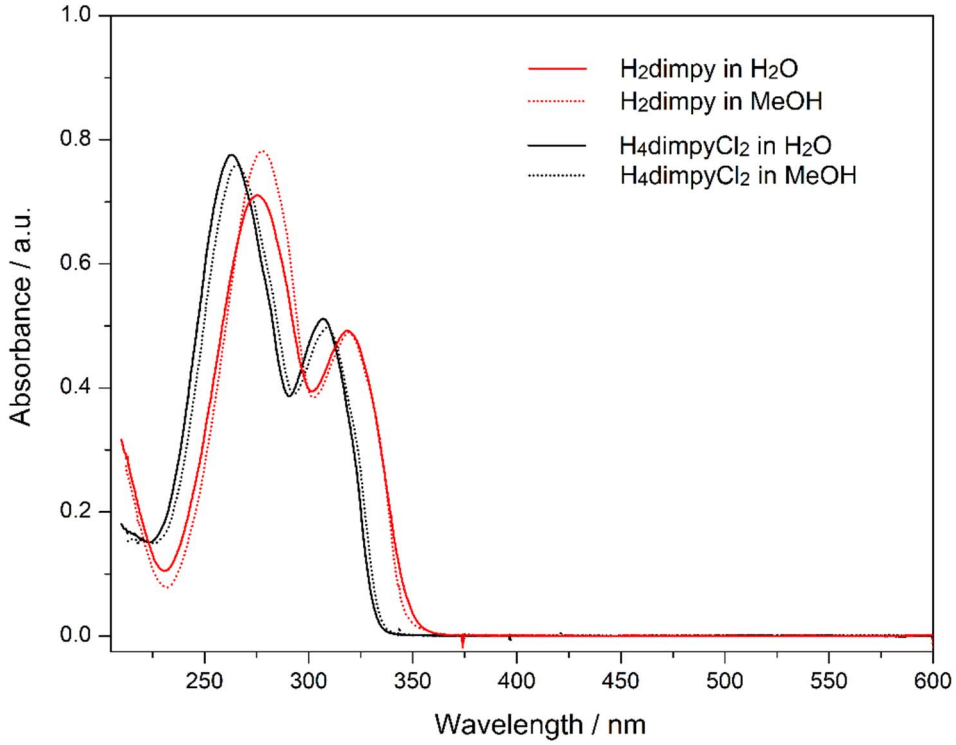


**Figure S3** UV-vis absorption spectra of a $2.8\times10^{-5}$ M solution of $H_2$dimpy (red) and $H_4$dimpy$Cl_2$ (black) in methanol (dotted line) and in water (solid line).

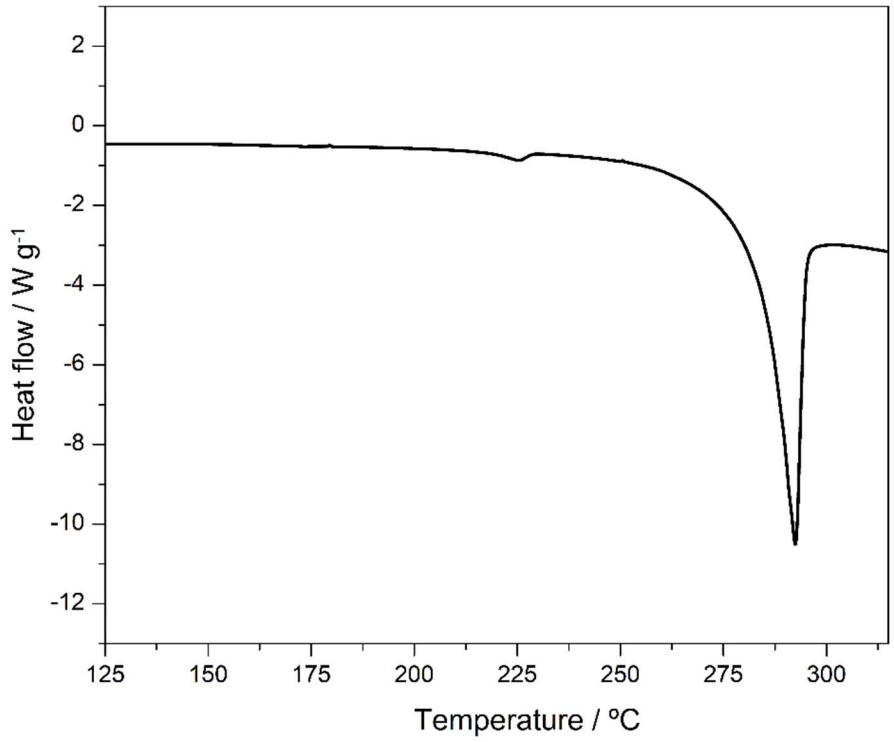


**Figure S4** DSC curve of $H_2$dimpy (m = 3.46 mg, 10 ºC $min^{-1}$) in nitrogen atmosphere.

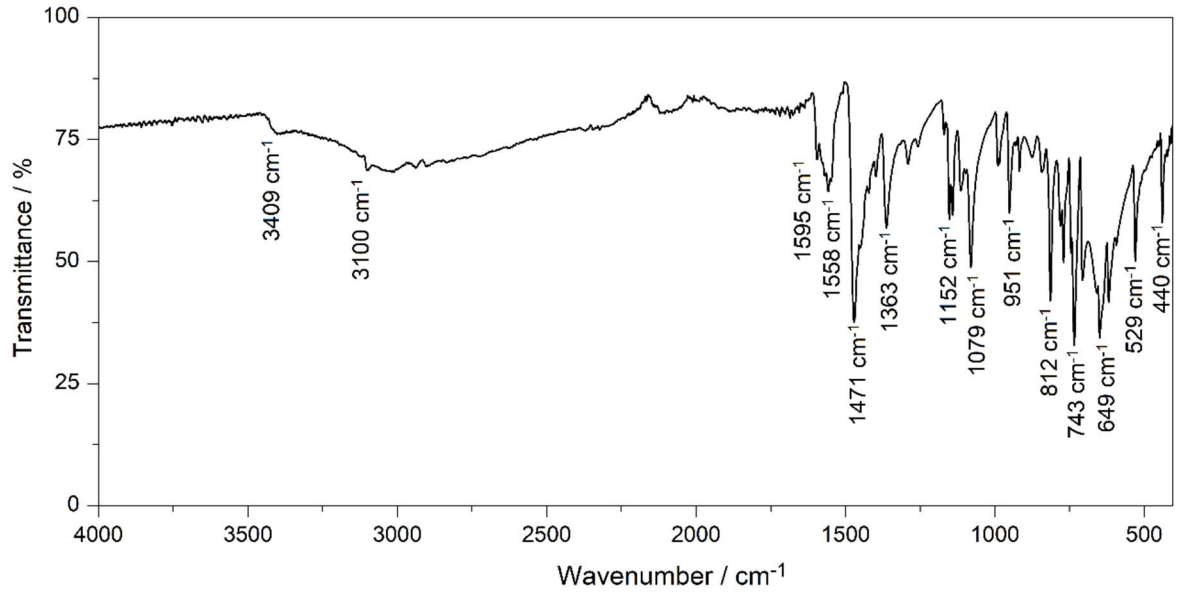


**Figure S5** FTIR-ATR spectrum of $H_2$dimpy.

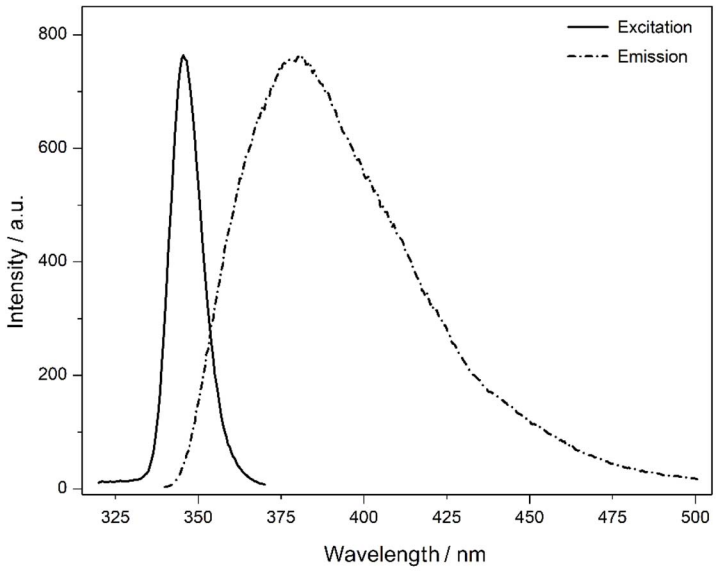


**Figure S6** Excitation (solid line) and emission (dashed-dot line) spectra of $H_2$dimpy in methanol ($2.5\times10^{-5}$ M).

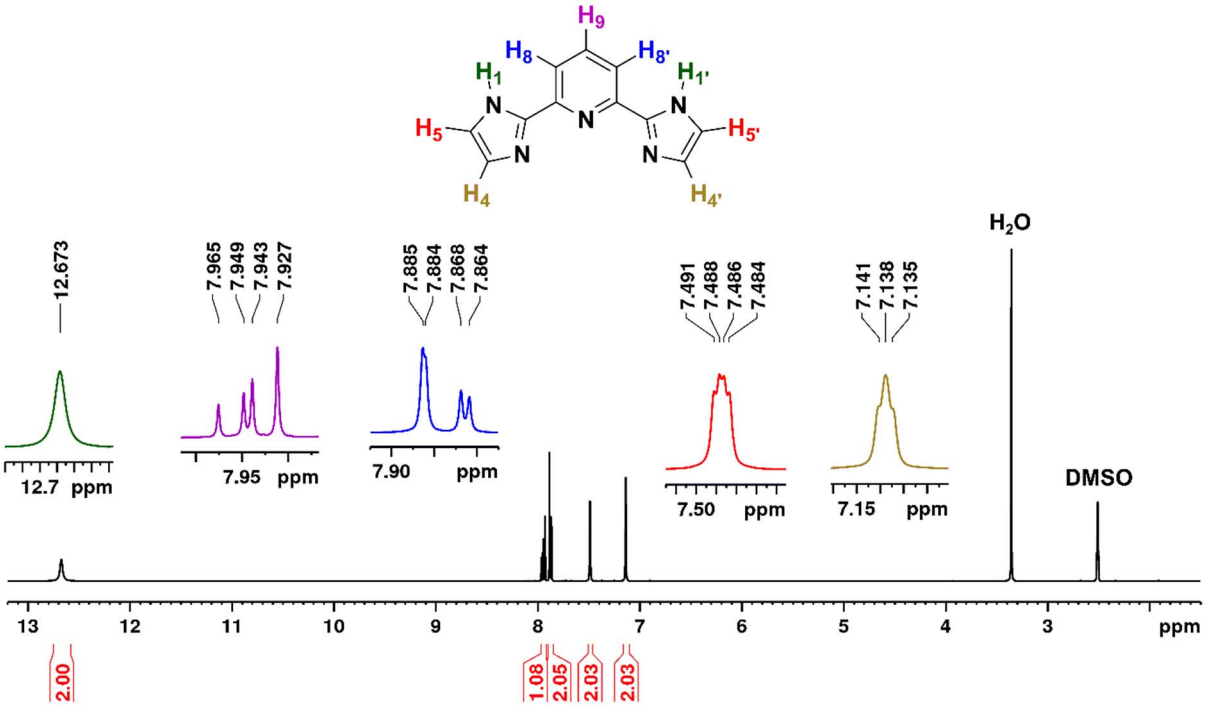


**Figure S7** $^1$H-NMR spectrum of $H_2$dimpy in DMSO-$d_6$ at 400 MHz.

The $^1$H-NMR spectrum (Fig. S7) is constituted by 5 signals that make reference to the 9 hydrogens present in the molecule $H_2$dimpy, being 4 pairs of hydrogens chemically equivalent as a consequence of the symmetry of the ligand. The most deshielded hydrogen ($H_1$, 12.67 ppm) is the one bound to the pyrrole-like nitrogen atom in the imidazole. The peak representing this hydrogen has the characteristic of showing a broad shape and a lower intensity if we compare it to the other peaks in the spectrum, and this happens because of the quadrupole moment of the nitrogen atom (Abraham & Bernstein, 1959).

Different peak attributions can be found in the literature regarding the $^1$H-NMR of $H_2$dimpy (Hammes *et al.*, 2005; Rigsby *et al.*, 2012; Ratier de Arruda *et al.*, 2017; Stupka *et al.*, 2004; Voss *et al.*, 2008), caused by the amount of water on the deuterated solvent, as shown in Fig. S8.

The effect of water content on the spectrum is shown by using two DMSO-$d_6$ solvents, one with a lesser amount of water (Fig. S8*(a)*) than the other (Fig. S8*(b)*). When these solvents were used to record $^1$H-NMR spectra of $H_2$dimpy, the results showed a much wider N–H peak for the solvent with a higher water content (Fig. S8*(d)*) than the drier solvent (Fig. S8*(c)*), as a consequence of a faster proton exchange (Ratier de Arruda *et al.*, 2017; Reddy *et al.*, 1962), shown in Scheme S1.

The use of a solvent with a small amount of water also lead to the distinction of the hydrogens $H_4$ ($\delta$ = 7.14 ppm) and $H_5$ ($\delta$ = 7.49 ppm) in the imidazole moiety of the molecule, which could not be observed when a solvent with a large quantity of water was used, due to hydrogens equivalence resulting in a singlet broad peak, as shown in Fig. S8*(d)*.

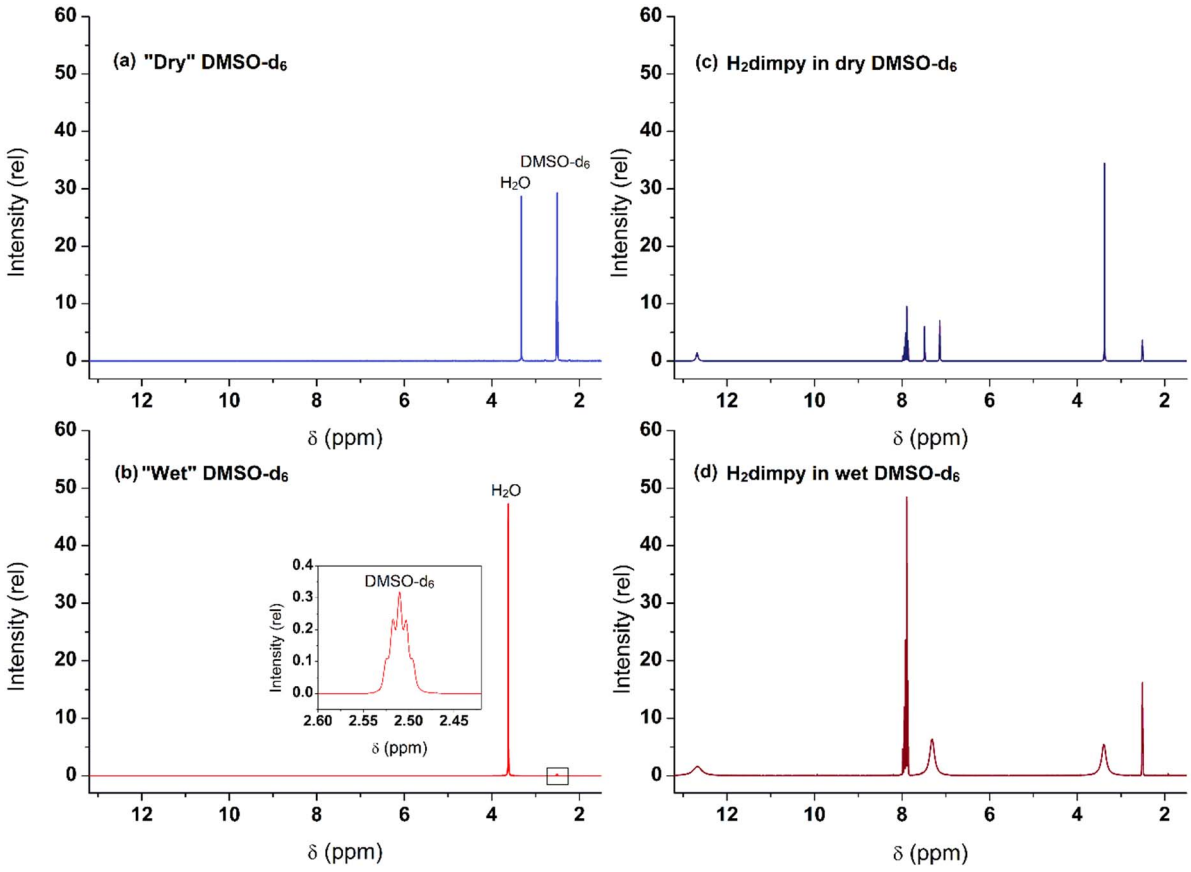


**Figure S8** $^1$H-NMR spectra displaying the peak patterns dependence on water content: Left: $^1$H-NMR spectra of DMSO-$d_6$ with *(a)* small water content and *(b)* a large water content. Right: $^1$H-NMR spectra of $H_2$dimpy in DMSO-$d_6$ with *(c)* a small water content and *(d)* a large water content.

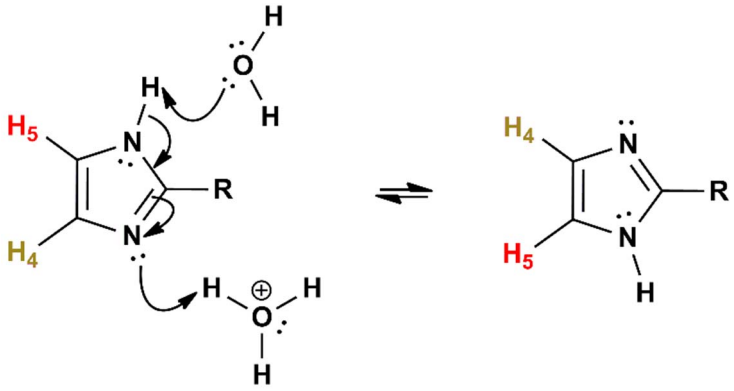


**Scheme S1** Proton exchange with water, leading to the equivalence of $H_4$ and $H_5$.

With this non-equivalence of the C–H hydrogens in mind, we acquired the 2D COSY spectrum of the $H_2$dimpy (Fig. S9). According to this spectrum, there is a strong interaction of the hydrogen $H_1$ with both $H_4$ and $H_5$ in the imidazole moiety confirming the proton exchange. Furthermore, it shows us that there is greater interaction with one of them, and this hydrogen $H_5$ is located in the downfield region of the spectrum (δ = 7.49 ppm).

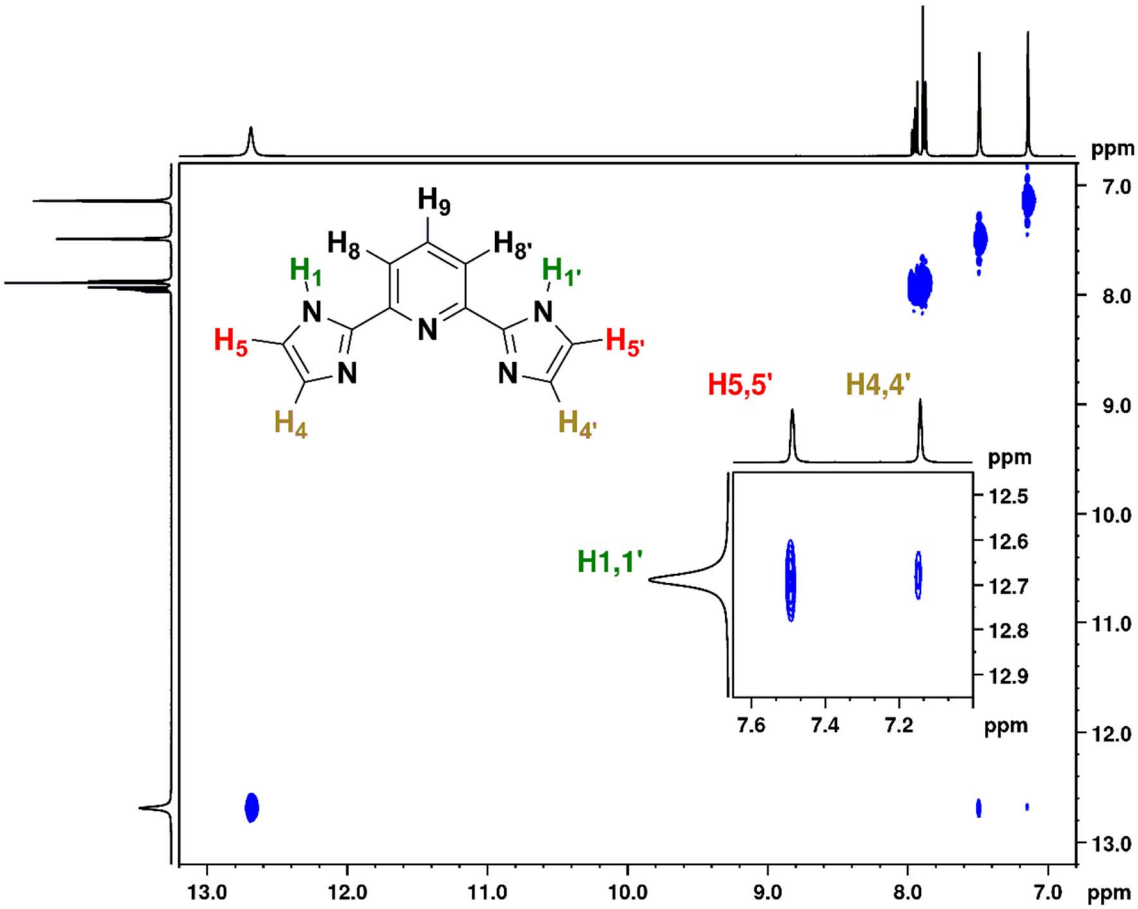


**Figure S9** $^1$H-$^1$H COSY spectrum of $H_2$dimpy acquired in DMSO-$d_6$.

This attribution is related to a lower electron density around the hydrogen $H_5$ as a consequence of the greater inductive effect made by the positive charged pyrrole-like nitrogen than by the nitrogen with the lone pair of electrons, as can be visualized in the resonant structures of the imidazole of the $H_2$dimpy molecule on Scheme 2.

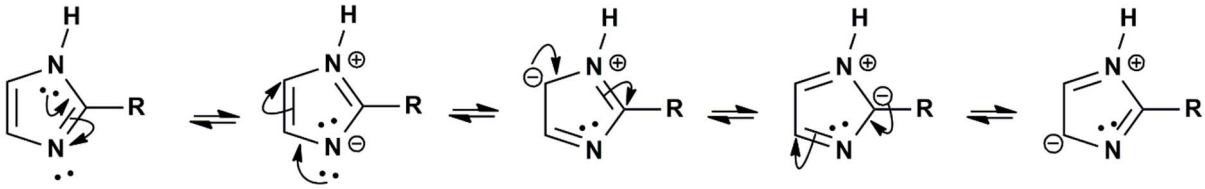

**Scheme S2** Resonance structures in the imidazole group of $H_2$dimpy.

The peaks attributed to $H_8$ and $H_9$ hydrogens were catalogued as multiplets instead of doublet and triplet, respectively, due to a phenomenon called strong coupling that occurs between them because the values of the difference in chemical shift (Δν) and the coupling constant (J) that links them are similar in magnitude (Pople *et al.*, 1959). Changes in the intensities and positions of the peak lines are observed as these chemical shift difference and coupling constant vary as shown in Fig. S10.

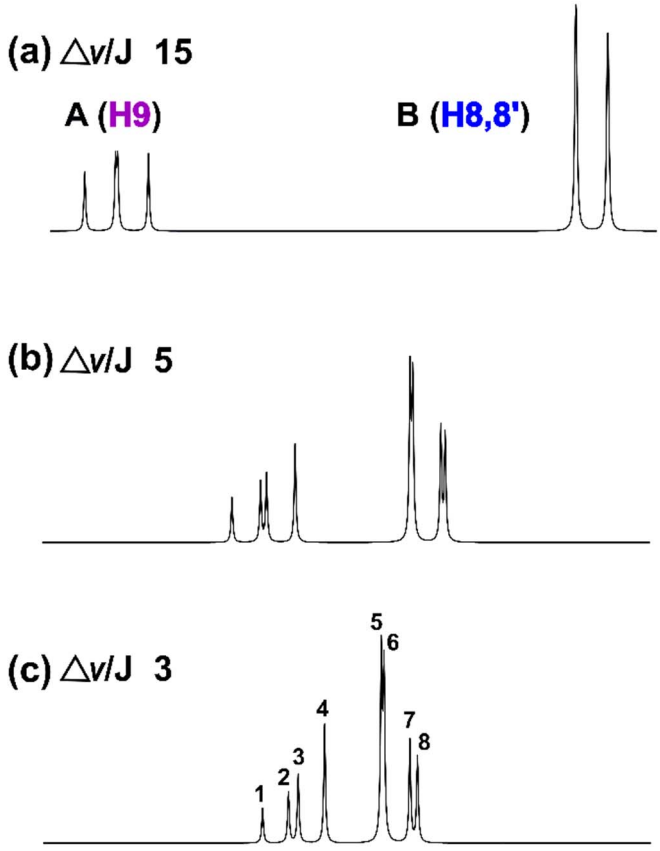


**Figure S10** Changes in peak patterns as ratio chemical shift difference/coupling constant varies. The spectra were obtained by using *WinDNMR* simulation software (Reich, 1995).

The chemical shift of $H_9$ is designated by line 3 and that of $H_8$ by the mean value of lines 5 and 7 (Pople *et al.*, 1959), resulting in 7.94 and 7.88 ppm, respectively. Being the chemical shift difference between them equal to 24 Hz and the coupling constant 7.85 Hz, the value of $\Delta\nu/J$ corresponds to 3, resulting in peak lines patterns very similar to that obtained by simulation.

The $^{13}$C-NMR spectrum (Fig. S11) shows 6 signals representing the 11 carbons of the $H_2$dimpy molecule, being 5 pairs of them chemically equivalent due to the symmetry of the molecule. The peaks assignment was done using the 2D HSQC spectrum (Fig. S12), which showed the direct interaction of the carbons attached to their respective hydrogens. $C_8$ is the most shielded carbon because it is located in the para-position in the pyridinic ring, while $C_9$ is less protected due to its *ortho*-position. $C_2$ and $C_7$ are the most downfield shifted carbons in the spectrum due to their position closer to the more electronegative nitrogen atoms (inductive effect), while $C_2$ being the most unprotected due to a greater inductive effect by being next to the two nitrogen atoms. A particular characteristic in the spectrum is the position of $C_4$ which is more deshielded than the $C_5$, in contrary to the expected, once $H_4$ is more shielded than the $H_5$. This characteristic is attributed to the deshielding character of the lone pair of electrons present in $N_3$ (Padilla-Martínez *et al.*, 1993), unlike $N_1$ which uses this pair of electrons to maintain the aromatic system of imidazole.

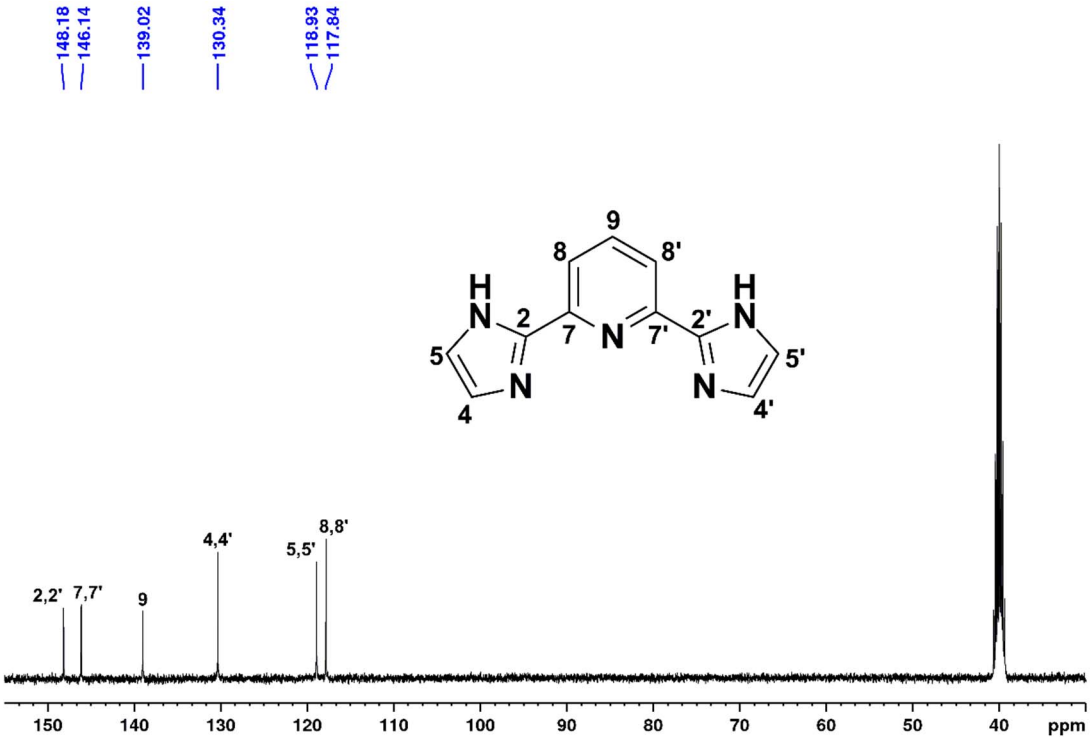


**Figure S11** $^{13}$C-NMR spectrum of $H_2$dimpy in DMSO-$d_6$.

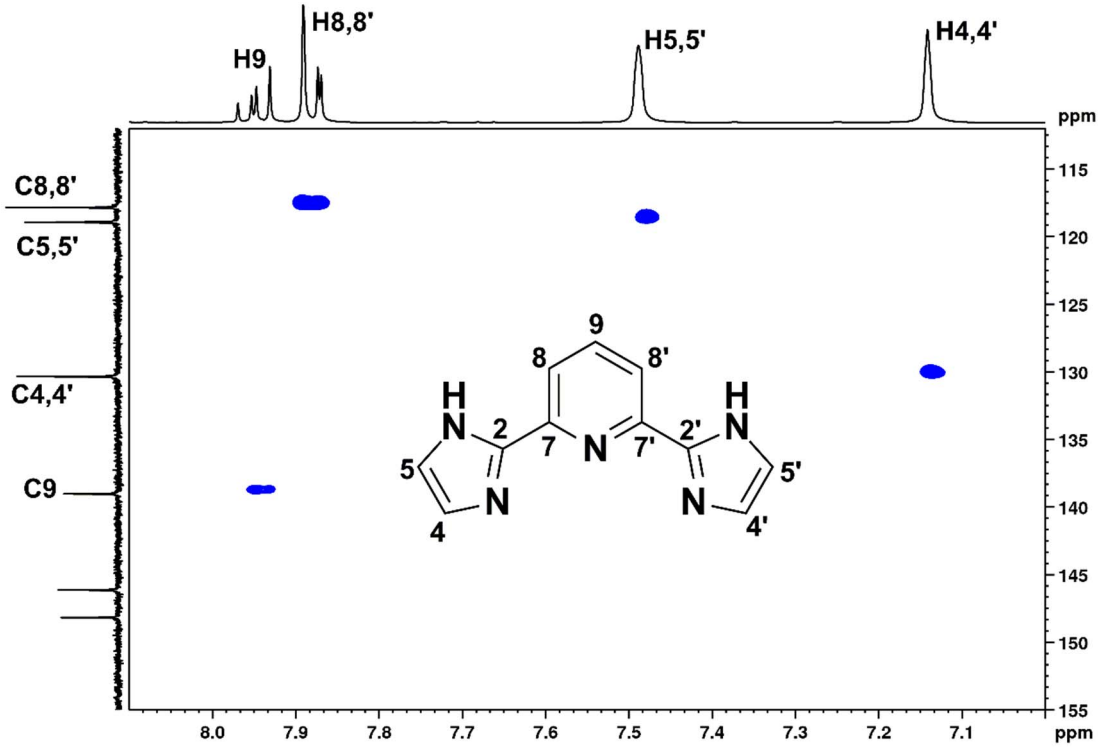


**Figure S12** $^{1}$H-$^{13}$C HSQC spectrum of $H_2$dimpy in DMSO-$d_6$.

### S1.4. p$K_a$ determination, electrochemical properties and DFT results

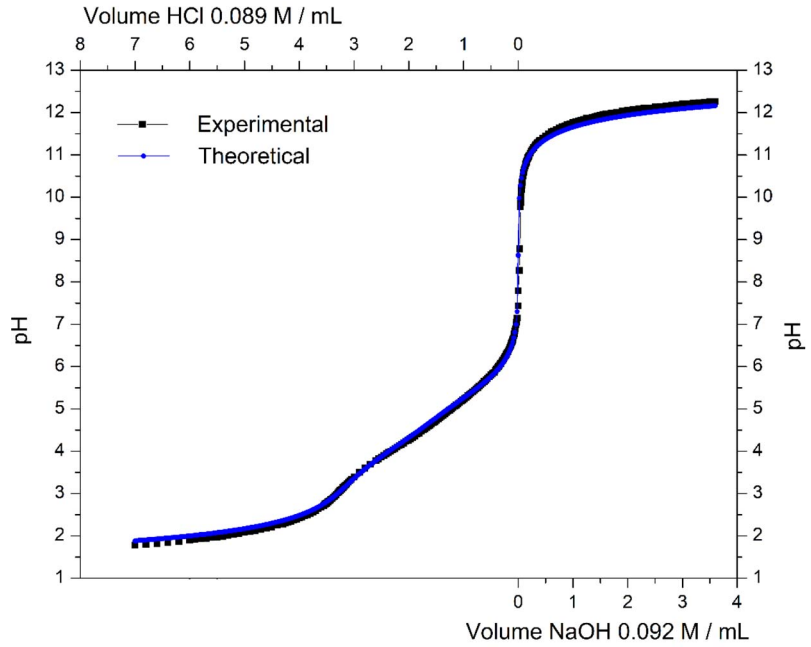


**Figure S13** Theoretical (blue) and experimental (black) potentiometric titration of $H_2$dimpy. The theoretical curve was simulated using *CurtiPlot* software (Gutz, 2018).

In Fig. S14 the absorption spectra of $H_2$dimpy during titration is divided into two regions, between pH 3-5 and pH 4.5-6.5. The p$K_a$ determination through spectrophotometric titration is made using the Henderson-Hasselbalch equation, wherein the concentrations of ionized species and non-ionized are equal, that is [$H_2$dimpy] = [$H_3$dimpy$^+$], and at this point, the measured pH will be equal to p$K_a$. For that, the variation of the absorbance maxima of each individual species ($H_2$dimpy and $H_3$dimpy$^+$) with the pH is plotted and the p$K_a$ value is obtained when the absorbance values converge, where [$H_2$dimpy] = [$H_3$dimpy$^+$]. However, due to the close p$K_a$ values, 3 species exist in a wide range of pH and so the determination of p$K_a$ using only spectrophotometric titration is very hard to achieve (Fig. S15). The lack of a well-defined isosbestic point in this case indicates the existence of at least two equilibria, which correspond to two protonations observed in the potentiometric titration.

The changes in the absorbance during the spectrophotometric titration shows that upon the first protonation the $\lambda_{max}$ of the $\pi$–$\pi^*$ transitions at 276 nm shifts hypsochromically with no changes on the extinction coefficient, while in the second protonation the hypsochromic shift is accompanied by an increase of 18% in the extinction coefficient. Using the p$K_a$ values, the speciation ($\alpha$) was calculated as shown in Fig. S16, yielding the expected spectra for each species in equilibrium shown in Fig. S17. The degree of the hypsochromic shift on the first protonation is bigger ($\Delta$ = 8 nm) than the observed in the second one ($\Delta$ = 5 nm) showing that the first protonation has a more important effect on the energy levels of the orbitals.

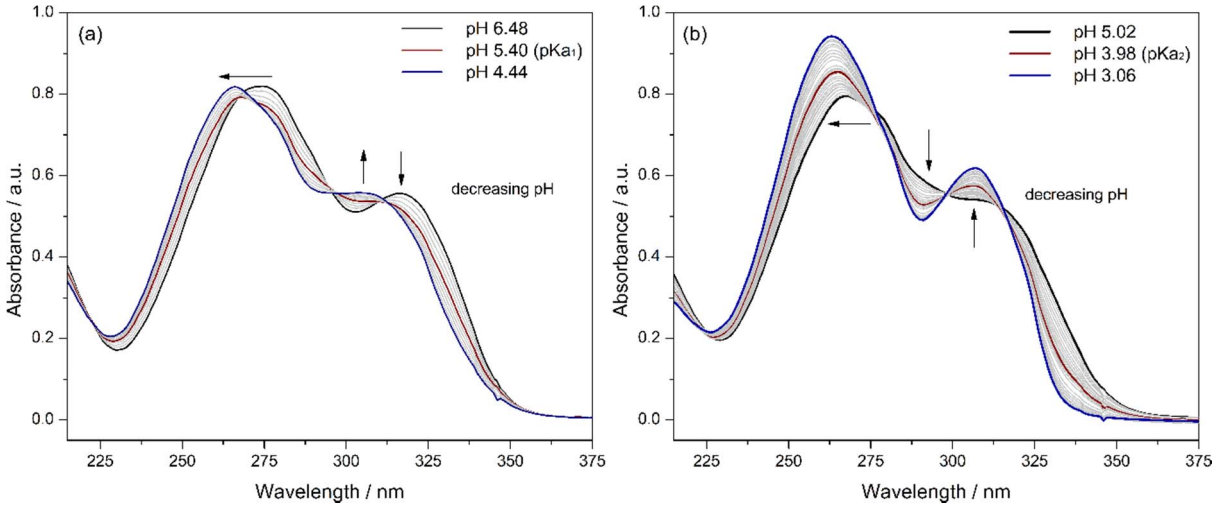


**Figure S14** UV-vis absorption spectra in an aqueous solution (5% methanol) of $H_2$dimpy ($3.5\times10^{-5}$ mol $L^{-1}$) during spectrophotometric titration at *(a)* pH 6.48–4.44 and *(b)* pH 5.02–3.06.

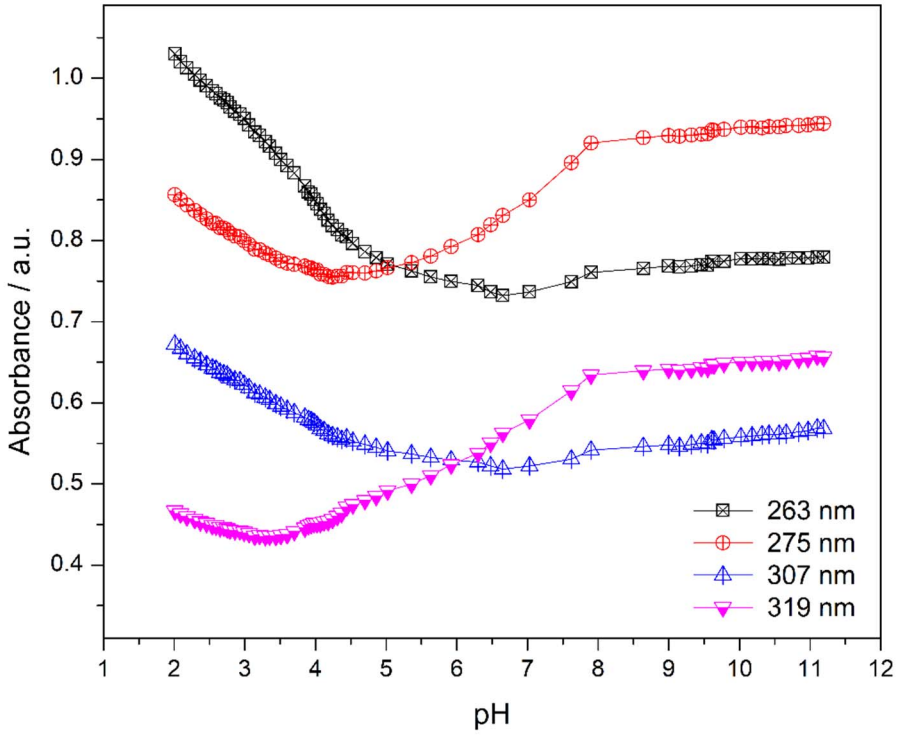


**Figure S15** Absorbance variation at various wavelengths as a function of pH during spectrophotometric titration in an aqueous solution of $H_2$dimpy ($3.5\times10^{-5}$ M).

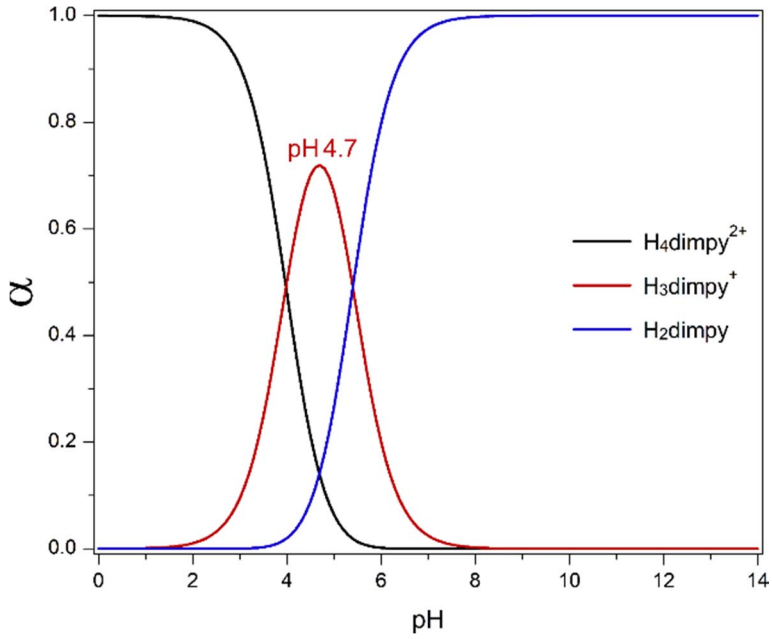


**Figure S16** Calculated speciation diagram based upon p$K_a$ values showing the pH dependence on the equilibrium concentration of [$H_4$dimpy$^{2+}$], [$H_3$dimpy$^{+}$] and [$H_2$dimpy].

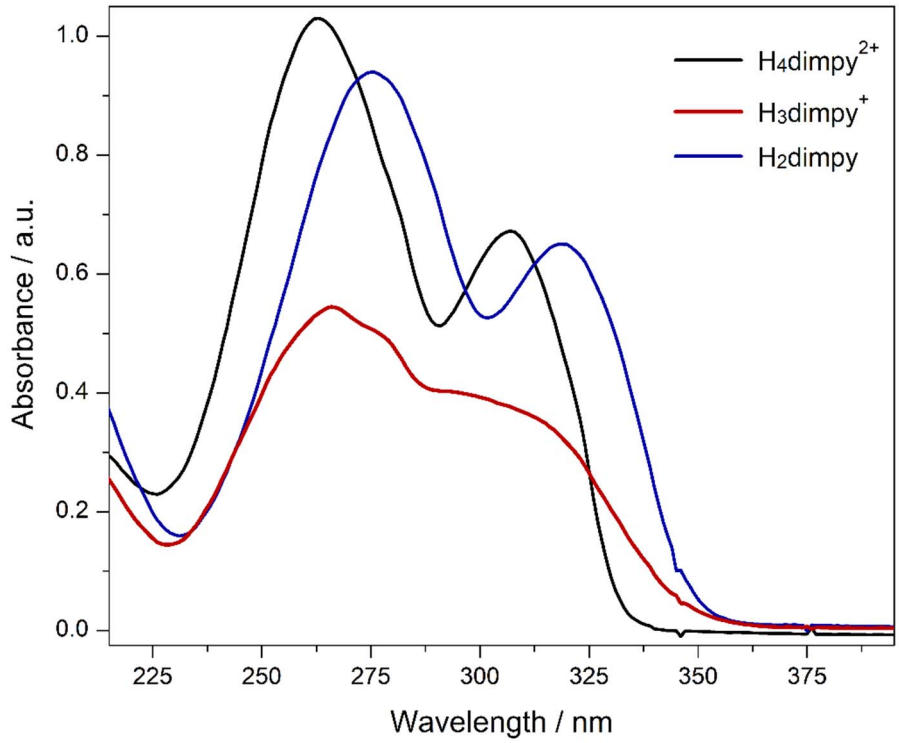


**Figure S17** UV-vis absorption spectra in aqueous solution of the species $H_4dimpy^{2+}$ (pH 2.01), $H_3dimpy^{+}$ (pH 4.70) and $H_2dimpy$ (pH 10.02). The spectrum of $H_3dimpy^{+}$ was obtained based on the calculated speciation, by subtracting the contribution of the two other species on the spectrum acquired.

The isodesmic strategy was used in the calculation of p$K_a$ values, in which a reference acid/base equilibrium is used in order to avoid the direct calculation of the absolute proton solvation energy using the following equations:

$$BH_{(aq)} + HCO_2^- \rightleftharpoons B^-_{(aq)} + HCO_2H \quad \Delta G^*_{(aq)}$$

$$pK_a(BH) = \frac{\Delta G*(aq)}{2.303\,RT} + pK_a(HCO_2H)$$

In the present work, formate/formic acid was selected as the reference together with several N-heterocyclic compounds in order to establish the calibration curve. Results are collected in Table S1 and Fig. S18.

**Table S1** Selected experimental and theoretical p$K_a$ values for the calibration curve.

| Molecule | Experimental | Theoretical |
|---|---|---|
| Formic acid | 3.77 | — |
| 4-$NO_2$-imidazole | -0.16 (p$K_{a1}$)<br>9.1 (p$K_{a2}$) | -5.47<br>8.94 |
| pyrazine | 0.6 | -2.59 |
| pyrimidine | 1.3 | -1.47 |
| 1,2,4-triazole | 2.2 | -1.05 |
| 6-$NO_2$-benzimidazole | 3.05 (p$K_{a1}$)<br>10.6 (p$K_{a2}$) | 0.08<br>10.89 |
| 4-Br-imidazole | 3.7 | -0.20 |
| pyridine | 5.2 | 3.72 |
| benzimidazole | 5.4 | 3.18 |
| imidazole | 6.9 | 5.01 |
| 4-$CH_3$-imidazole | 7.45 | 6.43 |
| 2-$CH_3$-imidazole | 7.75 | 6.27 |
| $H_4dimpy^{2+}$ | — | 0.43 |
| $H_3dimpy^{+}$ | — | 2.41 |
| $H_2dimpy$ | — | 16.51 |
| $H_4dimpy^{3+}$ | — | -14.71 |
| $H_3dimpy^{2+}$ | — | -2.72 |
| $H_2dimpy^{+}$ | — | 1.64 |

In order to calculate reduction potentials, we have used the following equations:

$$BH^{+}_{(aq)} + e^{-} \rightarrow BH_{(aq)}$$

$$\Delta G^0 = G(BH) - G(BH^+) - G(e^-)$$

$E = \left(-\frac{\Delta G^0}{F}\right) - E^0 ref$ in which F is the Faraday constant.

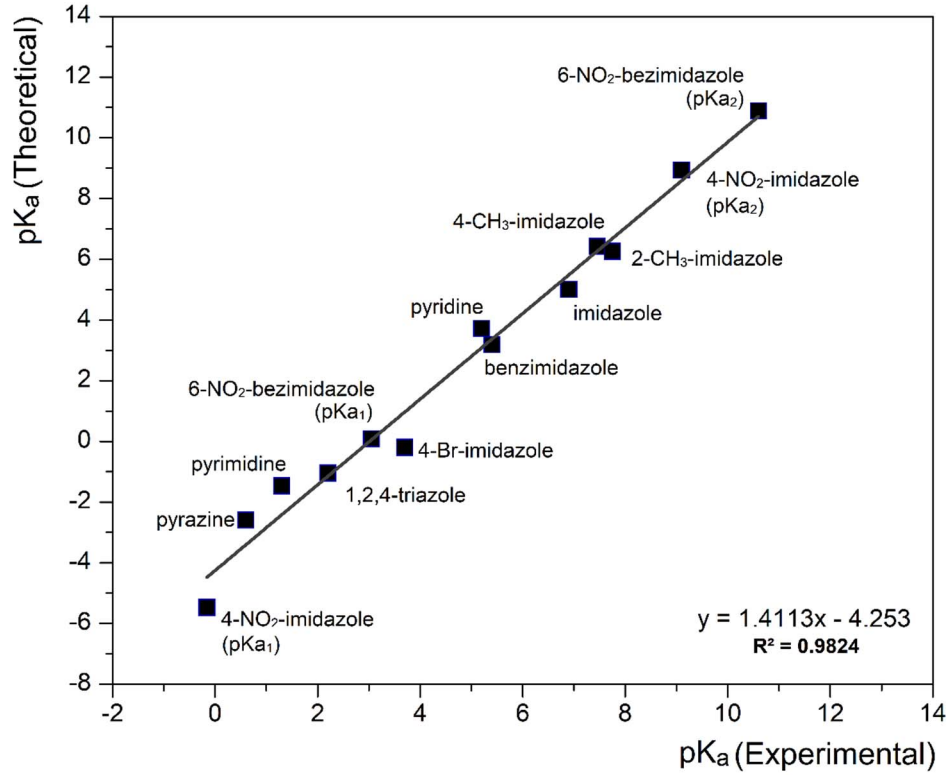


**Figure S18** Theoretical versus experimental p$K_a$ values for selected N-heterocyclic molecules.

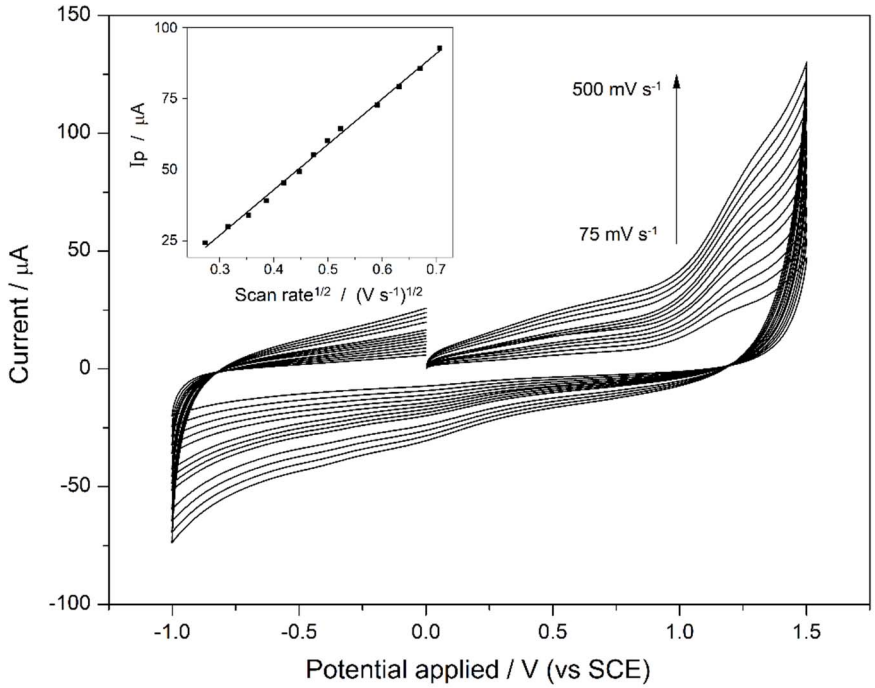


**Figure S19** Scan-rate-dependent CVs of $H_2$dimpy [1 mM] in water 4:1 methanol (pH 8.07, 0.1 M $KNO_3$). Inset: Dependence of the peak current ($I_p$) on the square root of the scan rate $v^{1/2}$.

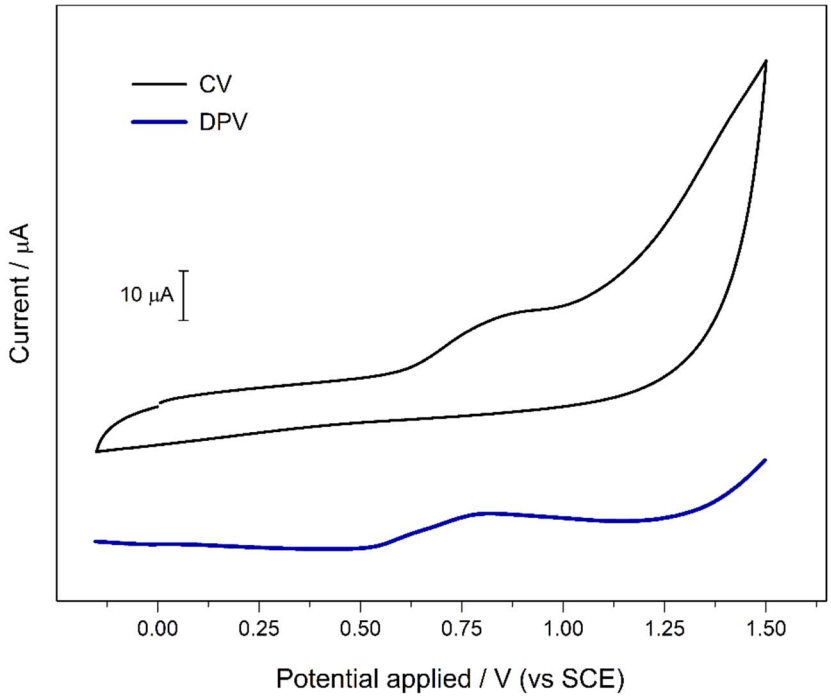


**Figure S20** CV (black) and DPV (blue) of $H_2$dimpy [1 mM] in aqueous solution (0.1 M B-R buffer, pH 11.08) recorded at 100 mV $s^{-1}$.

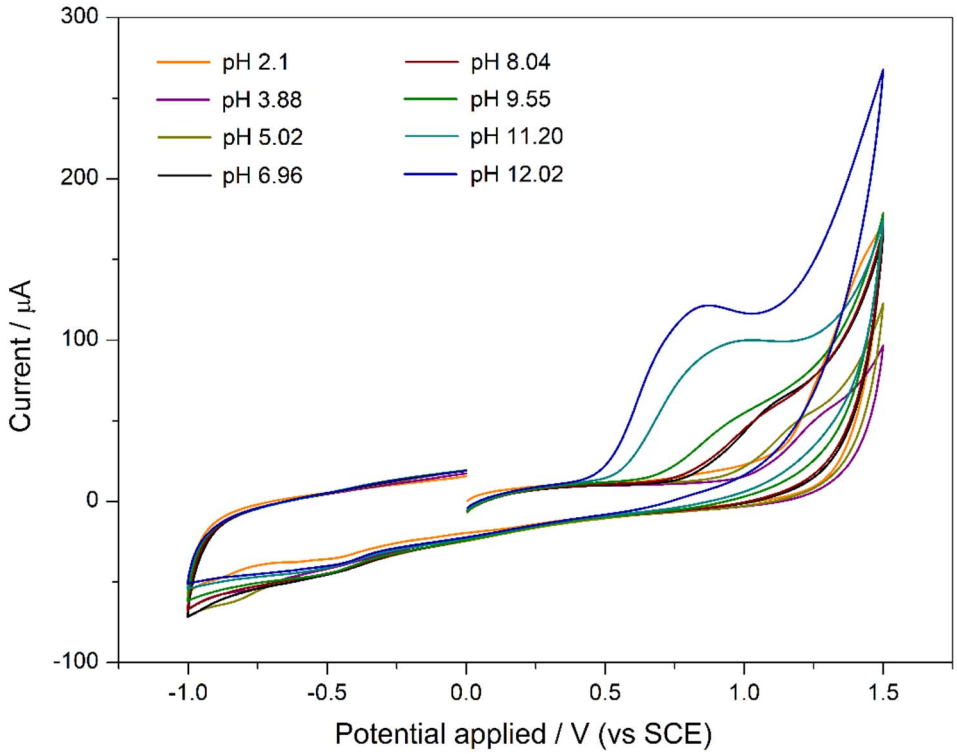


**Figure S21** CVs of $H_2$dimpy [1 mM] at 100 mV $s^{-1}$ in aqueous solution (0.1 M B-R buffer) under different pH conditions.

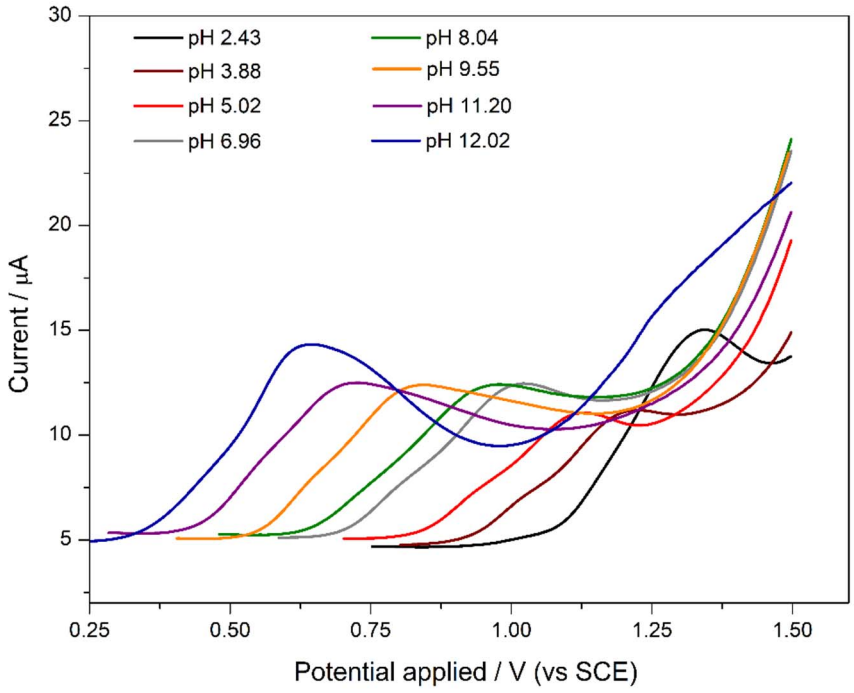


**Figure S22** DPVs of $H_2$dimpy [1 mM] at 100 mV $s^{-1}$ in aqueous solution (0.1 M B-R buffer) under different pH conditions.

DFT results shown in Eq. 1-3 are in good agreement with the oxidation potential observed in Fig. S21 and Fig. S22, because the theoretical reduction potentials for the first oxidation are also dependent on the protonation state of the molecule.

$H_3dimpy^{2+}_{(aq)} + e^- \rightarrow H_3dimpy^{+}_{(aq)}$ $E^0 = 1.48$ V (vs. SCE) (1)

$H_2dimpy^{+}_{(aq)} + e^- \rightarrow H_2dimpy_{(aq)}$ $E^0 = 1.18$ V (vs. SCE) (2)

$Hdimpy_{(aq)} + e^- \rightarrow Hdimpy^{-}_{(aq)}$ $E^0 = 0.30$ V (vs. SCE) (3)

As it is expected, deprotonation decreases the reduction potential, in very good agreement with the experimental results. For example, the peak potential at pH 7 in the experimental CV is observed at 1.015 V and is predicted by DFT at 1.18 V (Eq. 2). If one considers the effect of the oxidation in the p$K_a$ values, this also corroborates the experimental data since oxidation decreases the p$K_a$ values by several pH units yielding –7.4, 1.1 and 4.2 for the theoretical p$K_a$ of $H_4dimpy^{3+}$, $H_3dimpy^{2+}$, and $H_2dimpy^{+}$, oxidized species respectively. Together with the theoretical reduction potentials, this confirms that the complex pH dependence of the oxidation potential is due to the rich proton-coupled electrochemistry of the system.

A deeper electrochemical study is very hard to achieve for this system, since 2 protons and 2 electrons transfer processes on the $H_2$dimpy molecule gives rise to 9 different species with different oxidation states and protonation sites, considering only the oxidation process in acid media. When all the four protons and four electron oxidation and reduction process are considered, twenty-five independent species arise (Akutagawa & Saito, 1995; Okamura *et al.*, 2012), showing the complexity of this system.

The irreversible electrochemical behaviour was first thought to be related to the decomposition of the molecule upon oxidation since if the formation of a different species occurred (e.g. via N–H substitution, dimerization, etc. after deprotonation) a new oxidation peak should appear in a simple cycling experiment, which was not observed. However, since this new species could not be electrochemically active in these conditions, this led us to further investigate this oxidation process using spectroelectrochemical experiments, which confirmed the decomposition of $H_2$dimpy, however with no new bands being observed in the spectra upon oxidation. Instead, only the vanishing of the absorbance from π–π* bands can be noticed in both acid (Fig. S23) and basic (Fig. S24) media, suggesting that the decomposition is taking place with oxidation.

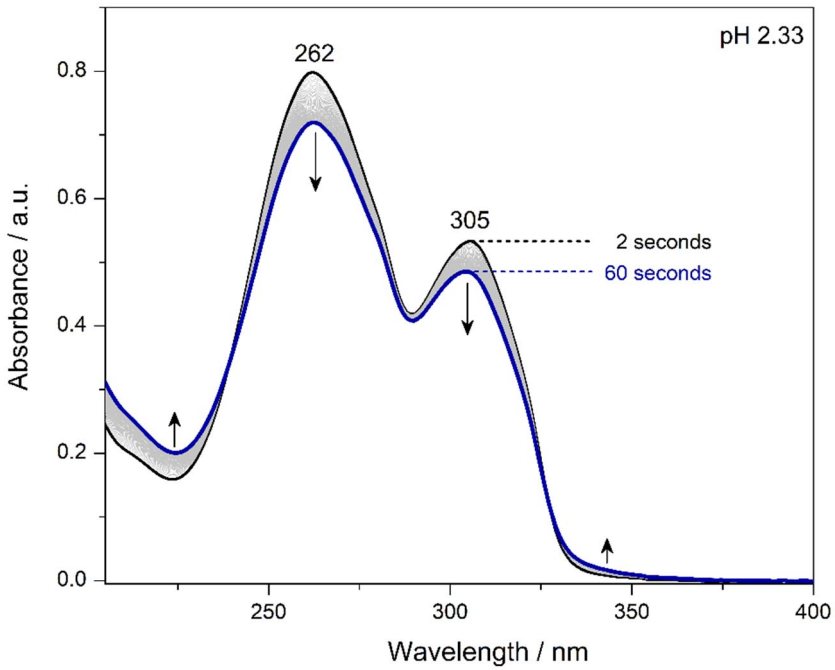


**Figure S23** Spectroelectrochemical measurement showing the UV-vis absorption spectra response during the first 60 seconds of controlled potential electrolysis at 1.3 V (vs SCE) of $H_2$dimpy ($3.5\times10^{-4}$ M) in aqueous solution (pH 2.33, 0.1 M KCl).

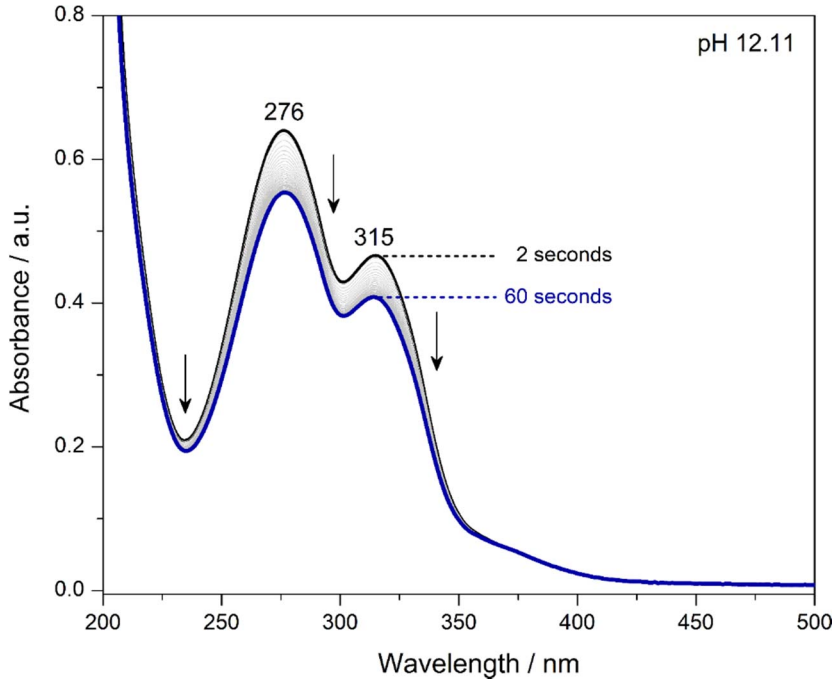


**Figure S24** Spectroelectrochemical measurement showing the UV-vis absorption spectra response during the first 60 seconds of controlled potential electrolysis at 0.8 V (vs SCE) of $H_2$dimpy ($3.5\times10^{-4}$ M) in aqueous solution (pH 12.11, 0.1 mol $L^{-1}$ KCl).

The combination of electrochemical, spectroelectrochemical and theoretical results suggests that the overall electrochemical behaviour of this molecule can be explained by a mechanism with successive proton-coupled electron transfer reactions, protonation equilibria and coupled chemical reactions. These consecutive reactions can be represented as in Equations 4-9, assuming pH 1.

$$H_4dimpy^{2+}_{(aq)} + H_2O_{(l)} \rightleftharpoons H_3dimpy^{+}_{(aq)} + H_3O^{+}(aq) \quad (4)$$

$$H_4dimpy^{2+}_{(aq)} + H_2O_{(l)} \rightarrow H_3dimpy^{2+}_{(aq)} + H_3O^{+}_{(aq)} + e^{-} \quad (5)$$

$$H_3dimpy^{2+}_{(aq)} \rightarrow \text{by-products of decomposition} \quad (6)$$

$$H_3dimpy^{2+}_{(aq)} + H_2O_{(l)} \rightleftharpoons H_2dimpy^{+}_{(aq)} + H_3O^{+}_{(aq)} \quad (7)$$

$$H_2dimpy^{+}_{(aq)} + H_2O_{(l)} \rightarrow Hdimpy^{+}_{(aq)} + H_3O^{+}_{(aq)} + e^{-} \quad (8)$$

$$Hdimpy^{+}_{(aq)} \rightarrow \text{by-products of decomposition} \quad (9)$$

## References

Abraham, R. J. & Bernstein, H. J. (1959). *Can. J. Chem.* **37**, 1056–1065.

Akutagawa, T. & Saito, G. (1995). *Bull. Chem. Soc. Jpn*. **68**, 1753–1773.

Gutz, I. G. R. (2018). *CurTiPot 4.3.0*. University of São Paulo, Brazil, http://www.iq.usp.br/gutz/Curtipot_.html.

Hammes, B. S., Damiano, B. J., Tobash, P. H., Hidalgo, M. J. & Yap, G. P. A. (2005). *Inorg. Chem. Commun.* **8**, 513–516.

Hashiguchi, B. G., Young, K. J. H., Yousufuddin, M., Goddard III, W. & Periana, R. A. (2010). *J. Am. Chem. Soc.* **132**, 12542–12545.

Okamura, M., Yoshida, M., Kuga, R., Sakai, K., Kondo, M. & Masaoka, S. (2012). *Dalton Trans.* **41**, 13081–13089.

Padilla-Martínez, I. I., Ariza-Castolo, A. & Contreras, R. (1993). *Magn. Reson. Chem.* **31**, 189–193.

Pople, J. A., Schneider, W. G. & Bernstein, H. J. (1959). *High-Resolution Nuclear Magnetic Resonance*, edited by W. C. Fernelius, L. P. Hammet, D. N. Hume, J. D. Roberts & H. H. Williams, pp. 123-128. New York: McGraw-Hill Book Company.

Ratier de Arruda, E. G., Farias, M. A., Jannuzzi, S. A. V., Gonsales, S. A., Timm, R. A., Sharma, S., Zoppellaro, G., Kubota, L. T., Knobel, M. & Formiga, A. L. B. (2017). *Inorganica Chim. Acta.* **466**, 456–463.

Reddy, G. S., Hobgood Jr., R. T. & Goldstein, J. H. (1962). *J. Am. Chem. Soc.* **84**, 336–340.

Reich, H. J. (1995). *J. Chem. Educ.* **72**, 1086.

Rigsby, M. L., Mandal, S., Nam, W., Spencer, L. C., Llobet, A. & Stahl, S. S. (2012). *Chem. Sci.* **3**, 3058–3062.

Stupka, G., Gremaud, L., Bernardinelli, G. & Williams, A. F. (2004). *Dalton Trans.* **3**, 407–412.

Voss, M. E., Beer, C. M., Mitchell, S. A., Blomgren, P. A. & Zhichkin, P. E. (2008). *Tetrahedron.* **64**, 645–651.